

Predicting CSI Sequences With Attention-Based Neural Networks

Valentina Rizzello, Benedikt Böck, Michael Joham, Wolfgang Utschick
 School of Computation, Information and Technology, Technical University of Munich, Germany
 {valentina.rizzello, benedikt.boeck, joham, utschick}@tum.de

Abstract—In this work, we consider the problem of multi-step channel prediction in wireless communication systems. In existing works, autoregressive (AR) models are either replaced or combined with feed-forward neural networks (NNs) or, alternatively, with recurrent neural networks (RNNs). This paper explores the possibility of using sequence-to-sequence (Seq2Seq) and transformer neural network (TNN) models for channel state information (CSI) prediction. Simulation results show that both, Seq2Seq and TNNs, represent an appealing alternative to RNNs and feed-forward NNs in the context of CSI prediction. Additionally, the TNN with a few adaptations can extrapolate better than other models to CSI sequences that are either shorter or longer than the ones the model saw during training.

Index Terms—Deep learning, transformer neural networks, sequence-to-sequence models, recurrent neural networks, autoregressive models, channel prediction

I. INTRODUCTION

CHANNEL prediction is crucial for time-varying channels. The problem of channel prediction is quite straightforward when the channel dynamics are known. In particular, when the Doppler frequency is known, linear predictors such as AR models or a Kalman Filter (KF) can effectively be used for tracking the CSI, see [1]–[4]. However, in a typical wireless communication system, the mobile terminals (MTs) move with different velocities and unknown channel statistics. Therefore, a finite number of AR predictors need to be pre-trained for different Doppler frequencies and the channel statistics must be estimated from the available data. In order for this approach to work well both *i*) the Doppler frequency must be correctly estimated, and *ii*) a potentially large number of linear predictors need to be stored. Additionally, a wrong or a coarse approximation of the Doppler frequency can cause a non-negligible loss in practice.

In recent years, NNs have become a promising solution in various research fields including wireless communications. In [5], convolutional neural networks (CNNs) are used in combination with AR models for CSI forecasting. In particular, CNNs are used to correctly identify the channel dynamics, and to load the corresponding pre-trained AR predictor to forecast the CSI. The authors of [6] also propose a hybrid

This work was supported by an unrestricted gift from Futurewei Technologies, Inc., USA.

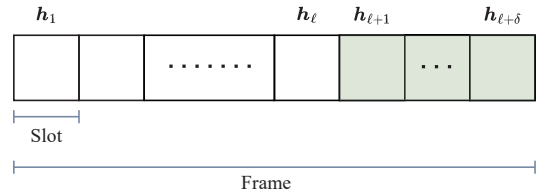


Figure 1. Frame structure.

approach called Hypernetwork Kalman Filter. There, a single-antenna setup is considered and only Kalman equations are utilized for prediction, whereas a hypernetwork continuously updates the Kalman parameters based on past observations. The work in [7] instead considers frequency-selective channels and optimizes linear predictors by leveraging a long-short-term channel decomposition, in which the channel is decomposed into long-term space-time signatures and fading amplitudes. Additionally, meta-learning is used for training the model and reducing the required number of pilots. Another popular idea adopted by [5], [8], [9] is to use more sophisticated NNs, namely, RNNs for CSI prediction. In particular, due to the ability of RNNs to incorporate the dynamics typical of time series data, they are considered a valid alternative to AR models for time series forecasting. However, notably RNNs are difficult to train due to vanishing or exploding gradient issues, see [10]. Among the recent advances, we find the work in [11] where the CSI prediction is incorporated in a reinforcement learning-based setup where the goal is to maximize the multi-user sum rate over time. In this setting, the so-called Actor Network is responsible for CSI prediction and it is realized via a multi-layer perceptron (MLP). In this work, we evaluate different models on a multi-step channel prediction task, where the users are moving with unknown velocities, and where a wide range of velocities is covered. The models considered in this work include AR models, feed-forward NNs, such as MLPs and models specifically designed for sequential data, such as long-short-term memory (LSTM), Seq2Seq, and the most recent TNN models [12]. Motivated by the success in natural language processing and by the exciting results achieved by TNNs, we hereby adopt this architecture to accomplish the CSI prediction task. In [13], a method based on TNNs has been developed for CSI prediction. However, differently from our

method, the prediction of the CSI sequence is done in parallel, instead of sequentially. In [13], the authors argue that this technique avoids prediction error propagation. On the contrary, with our simulations, we show that the sequential prediction outperforms the parallel prediction. Additionally, we evaluate the robustness of the sequential models to sequence lengths, other than the ones assumed for training. In the meanwhile, TNNs have been used in wireless communications for realizing autoencoders in the context of CSI feedback generation in frequency division duplex (FDD) systems, see [14]–[16]. In [17], TNNs are adapted to time series data in the context of influenza-like illness forecasting. However, in [17], only univariate data are used, and the plain transformer architecture proposed by [12] is used. In this work, instead, we propose non-negligible changes to the original architecture to allow the model to extrapolate the CSI sequences that are either shorter or longer than the ones the model saw during training.

Hence our contributions can be summarized as follows:

- we introduce two new models, namely Seq2Seq and TNN, that exploit the attention mechanism for CSI prediction;
- we show that the proposed models, and in particular, the TNN model, outperform existing models and exhibit solid performance gains also when tested on sequence lengths, other than the ones considered during the training.

The rest of the paper is organized as follows. In Section II, the system model is described; in Section III, we present in detail the different models that are used in this work; in Section IV, the dataset used and the training setup are presented, and the simulation results are discussed; in Section V, we draw our conclusions.

II. SYSTEM MODEL

We consider a base station (BS) serving multiple MTs in a typical 5G cell. The BS is equipped with M antennas, whereas the single-antenna users are moving with different velocities and, therefore, experience different fading conditions. In particular, we assume that the velocities of the users are constant within the duration of a frame. Additionally, as depicted in Fig. 1, we assume that the channel remains constant for the duration of a slot which we denote as T_{slot} , and that a frame contains N_{slot} slots. From now on, we denote as $\mathbf{h}_i \in \mathbb{C}^M$ the CSI corresponding to the i th generic slot of the CSI time series. The goal of multi-step CSI prediction is to predict the next δ CSI vectors by assuming the previous ℓ CSI as known. In a simplified notation, that omits the explicit notation of the time series character, we write

$$\mathbb{C}^M \ni \mathbf{h}_{\ell+k} = f(\mathbf{h}_1, \dots, \mathbf{h}_\ell; k), \quad k = 1, \dots, \delta, \quad (1)$$

where f denotes a generic function that can be used for prediction. Within this work, we assume that the channel $\mathbf{h}_i \quad i = 1, \dots, \ell$ is not perfectly known, but that only the last ℓ noisy observations of the recent channels are available, that is,

$$\mathbf{h}_i \leftarrow \mathbf{h}_i + \mathbf{n}_i \quad i = 1, \dots, \ell, \quad (2)$$

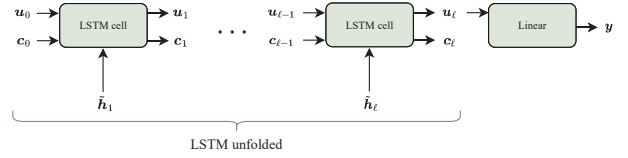


Figure 2. LSTM model.

where \mathbf{n}_i denotes the complex-valued noise vector with elements distributed as $\mathcal{CN}(0, \sigma_n^2)$.

III. MODELS DESCRIPTIONS

A. MAR model

One possible solution to the prediction problem is to fit δ multivariate autoregressive (MAR) models as

$$\mathbf{h}_{\ell+k}^T = \sum_{j=1}^{\ell} \mathbf{h}_j^T \Phi_j^{(k),T} + \epsilon^{T,(k)}, \quad k = 1, \dots, \delta, \quad (3)$$

where $\Phi_j^{(k),T} \in \mathbb{C}^{M \times M}$ denotes the j -th parameter of the k -th AR model, and $\epsilon^{T,(k)}$ is a noise terms that models everything that cannot be captured by the AR components. Therefore, in order to minimize the error, the parameters can be found with the classic least squares (LS) regression. In particular, by assuming that our dataset contains N_{train} training samples, we obtain the parameters as

$$\begin{aligned} [\Phi_1^{(k)}, \dots, \Phi_\ell^{(k)}]^T &= \mathbf{A}^\dagger [\{\mathbf{h}_{\ell+k}\}_1, \dots, \{\mathbf{h}_{\ell+k}\}_{N_{\text{train}}}]^T, \\ \text{where } \mathbb{C}^{N_{\text{train}} \times M\ell} \ni \mathbf{A} &= \begin{bmatrix} \{\mathbf{h}_1^T\}_1 & \dots & \{\mathbf{h}_\ell^T\}_1 \\ \vdots & \ddots & \vdots \\ \{\mathbf{h}_1^T\}_{N_{\text{train}}} & \dots & \{\mathbf{h}_\ell^T\}_{N_{\text{train}}} \end{bmatrix}, \end{aligned}$$

with \mathbf{A}^\dagger denoting the pseudo inverse of the matrix \mathbf{A} .

B. MLP

Another possible approach is to train a MLP to predict the δ unknown CSI vectors given the ℓ known vectors. In a two-layer MLP, the neurons of the input layer are mapped first to the hidden layer, and then to the output layer. For simplicity in our work, we consider real-valued neural networks. Therefore, we transform the complex vector \mathbf{h}_i into a real vector where the real and imaginary parts of the original vector are concatenated, i.e.,

$$\mathbb{R}^{2M} \ni \tilde{\mathbf{h}}_i = \text{concat}(\Re(\mathbf{h}_i), \Im(\mathbf{h}_i)). \quad (4)$$

In this way, the input layer is represented by $\mathbf{x} = \text{concat}(\tilde{\mathbf{h}}_1, \dots, \tilde{\mathbf{h}}_\ell) \in \mathbb{R}^{2M\ell}$ whereas the output layer consists of $\mathbf{y} = \text{concat}(\tilde{\mathbf{h}}_{\ell+1}, \dots, \tilde{\mathbf{h}}_{\ell+\delta}) \in \mathbb{R}^{2M\delta}$. By denoting the weights and bias of the hidden layer and output layer as $\mathbf{W}_1, \mathbf{b}_1, \mathbf{W}_2, \mathbf{b}_2$ respectively, we obtain

$$\mathbf{y} = \mathbf{W}_2 \text{ReLU}(\mathbf{W}_1 \mathbf{x} + \mathbf{b}_1) + \mathbf{b}_2, \quad (5)$$

where the dimension of the parameters are chosen based on the dimension of the hidden layer, and ReLU denotes the

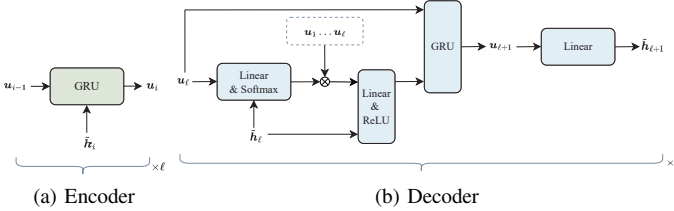


Figure 3. Seq2Seq model.

element-wise rectified linear unit activation function. Finally, we can recover the complex vectors $h_{\ell+1}, \dots, h_{\ell+\delta}$ by an appropriate reshaping of the vector y , and by performing the reverse operation of Eq. (4).

C. LSTM model

Differently from feed-forward NNs like MLPs, RNNs are sequence models designed specifically for sequential data. In traditional feed-forward NNs, all the inputs are processed once, instead, the recurrent structure of RNNs allows for the weights to be shared over all time steps of a sequence. Hence, the information is fed back to the same node multiple times, depending on the length of the sequence. In RNNs, the same function is applied to each input of the sequence in order to produce the corresponding output and hidden state. Since RNNs suffer from the vanishing and exploding problems, we consider a LSTM network which has been proposed to address exactly this limitation of RNNs, see [18]. The model is illustrated in Fig. 2. More in detail, a LSTM cell employs three different gates, an input gate i_t , a forget gate f_t , and an output gate o_t to prevent exploding or vanishing gradient. The main idea behind the gating system is not to retain information about all the inputs and to capture long-term dependencies. In formulas, we have:

$$\begin{aligned} i_t &= \sigma(\mathbf{W}_i \text{concat}(\tilde{h}_t, \mathbf{u}_{t-1}) + \mathbf{b}_i) \\ f_t &= \sigma(\mathbf{W}_f \text{concat}(\tilde{h}_t, \mathbf{u}_{t-1}) + \mathbf{b}_f) \\ o_t &= \sigma(\mathbf{W}_o \text{concat}(\tilde{h}_t, \mathbf{u}_{t-1}) + \mathbf{b}_o) \\ \tilde{c}_t &= \tanh(\mathbf{W}_{\tilde{c}} \text{concat}(\tilde{h}_t, \mathbf{u}_{t-1}) + \mathbf{b}_{\tilde{c}}) \\ c_t &= f_t \odot c_{t-1} + i_t \odot \tilde{c}_t \\ \mathbf{u}_t &= o_t \odot \tanh(c_t), \end{aligned} \quad (6)$$

where \mathbf{u}_t and c_t denote the hidden and the cell states, respectively. Note that differently from the classical RNN, where the next hidden state is directly represented by \tilde{c}_t , here, the hidden state is updated using the cell state c_t . Therefore, \tilde{c}_t is first modulated by the input gate and then by the output gate. Note that $\sigma(\cdot)$ denotes the sigmoid function whose output values are in the interval $[0, 1]$. In order to predict the CSI in the next δ slots, we considered a two-layer LSTM to encode the input sequence and a final linear layer that directly outputs the CSI of the next δ steps. In addition, the original CSI vector

h_i is transformed into real values as described in the previous subsection, see Eq. (4).

D. Seq2Seq model with attention

Another relevant framework to solve the problem at hand is the Seq2Seq architecture, see [19]. A Seq2Seq model has been thought for those cases in which both, the input and the output, are sequences. The model architecture is illustrated in Fig. 3 and it comprises of an *encoder* and a *decoder*. The encoder encodes the input sequence using an RNN, e.g., a gated recurrent unit (GRU). In formulas we can write:

$$\begin{aligned} \mathbf{z}_t &= \sigma(\mathbf{W}_z \text{concat}(\tilde{h}_t, \mathbf{u}_{t-1}) + \mathbf{b}_z) \\ \mathbf{r}_t &= \sigma(\mathbf{W}_r \text{concat}(\tilde{h}_t, \mathbf{u}_{t-1}) + \mathbf{b}_r) \\ \tilde{\mathbf{u}}_t &= \tanh(\mathbf{W}_{\tilde{u}} \text{concat}(\tilde{h}_t, \mathbf{r}_t \odot \mathbf{u}_{t-1}) + \mathbf{b}_{\tilde{u}}) \\ \mathbf{u}_t &= (\mathbf{1} - \mathbf{z}_t) \odot \tilde{\mathbf{u}}_t + \mathbf{z}_t \odot \mathbf{u}_{t-1}, \end{aligned} \quad (7)$$

where \mathbf{z}_t and \mathbf{r}_t represent the update and the reset gate, respectively. In particular, when \mathbf{z}_t is close to 1, we ignore completely the current input \tilde{h}_t for the update of the current hidden state \mathbf{u}_t . On the other hand, when both \mathbf{r}_t and \mathbf{z}_t are equal to zero, the hidden state only depends on the current input. Similarly to the LSTM, also in the GRU, the gating mechanism is employed such that the RNN can capture the long-term dependencies. The decoder also comprises a GRU. However, at each step, and in order to encourage the decoder to leverage the important parts of the encoder outputs before making the prediction, an attention mechanism with respect to the encoder outputs precedes the GRU [20]. The model used for the decoder is shown in Fig. 3b. In particular, the current hidden state, and the current input are concatenated, and then projected via a single layer onto a dimension equal to the number of encoder outputs ℓ . At this point, the obtained vector is normalized with the softmax(\cdot) function to obtain the weights (probabilities, or attention-scores) which are then used to scale the encoder outputs u_1, \dots, u_{ℓ} . Furthermore, this result is concatenated with the current input and passed through a linear layer followed by a ReLU to produce the input vector for the GRU. The first input of the decoder is represented by the last known CSI snapshot. Additionally, during training teacher-forcing [21] is used in the decoder, which means that during training we use the true noisy CSI observation as input for the next time step, instead of using the output predicted with the decoder. Finally, and analogously with typical RNNs, the output of the GRU is fed to a linear layer to output the prediction of the next CSI vector. Also in this case, we operate with real-valued CSI, by following the approach described in Subsection III-B.

E. TNN

A TNN consists of an *encoder* and a *decoder* NN. The model is illustrated in Fig. 4. The encoder has L_{enc} layers and each encoder layer contains two consecutive residual networks. The first residual network has the “multi-head attention” as

Algorithm 1 Multi-head attention

Input: $z \in \mathbb{R}^{\ell \times (Hd)}$, H , e , m
 ▷ e and m are used only for the decoder layers.

$$q \leftarrow zQ$$

if e **then**

$$k \leftarrow eK, v \leftarrow eV$$

else

$$k \leftarrow zK, v \leftarrow zV$$

end if

reshape q , k and v from $\ell \times (Hd)$ to $H \times \ell \times d$

for $h = 1$ to H **do**

$$p_h \leftarrow q_h k_h^T / \sqrt{d}$$

if m **then**

$$p_h \leftarrow m \odot p_h$$

end if

$$a_h \leftarrow \text{softmax}(p_h)v$$

end for

reshape a from $H \times \ell \times d$ to $\ell \times (Hd)$

Output: a

the main module of the residual block, whereas the second residual network contains an MLP as the main module. Moreover, the layer normalization (LN) [22] precedes each of these modules. The MLP contains two fully-connected layers and a GeLU [23] activation function after the first layer. For completeness, we describe the “multi-head attention” forward pass in the Algorithm 1, where the matrices Q , K , V denote the learnable parameters of the multi-head attention block, and H denotes the number of “heads” of the multi-head attention block. The decoder has L_{dec} layers and each layer contains three consecutive residual networks. The first and the second residual networks have the “multi-head attention” as the main module of the residual block, whereas the third residual network contains an MLP as the main module. As for the encoder layer, the LN precedes each of these modules. The main difference with respect to the encoder layer is in the structure of the “multi-head attention” block. In particular, for the first residual network of the decoder, Algorithm 1 takes as input, in addition to the main sequence z , a mask m that ensures that the prediction of the CSI for a certain slot only depends on previous slots. In the second residual network of the decoder, instead, Algorithm 1 takes as input the output sequence e obtained with the encoder NN in addition to the main sequence z . Following the same reasoning as for the Seq2Seq model, the last known snapshot \tilde{h}_ℓ becomes the first input of the decoder network. Similarly to the Seq2Seq model, also in this case, and only during training, we use the true noisy CSI observations $\tilde{h}_{\ell+1}, \dots, \tilde{h}_{\ell+\delta-1}$ as further decoder inputs, instead of the predicted ones obtained at the decoder output. Note that, similarly to the original implementation in [12] also in this case we transform the input sequence, in both, the encoder and the decoder, first by a linear layer and then by

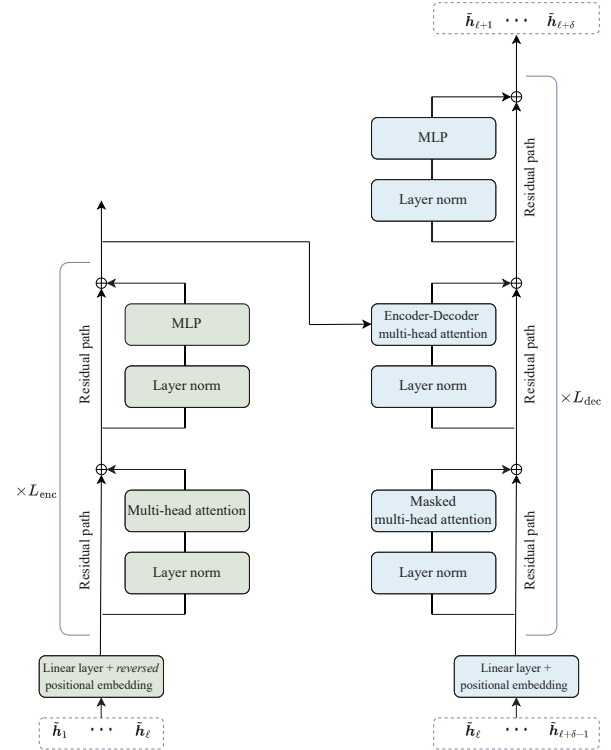


Figure 4. Transformer for CSI prediction. The encoder is on the left in green, and the decoder is on the right in blue.

adding a constant bias term, called positional embedding. The positional embeddings are constant, non-learnable vectors that are added after the first linear layer, and are constructed with sine and cosine functions. In particular, we used:

$$\begin{aligned} PE(j, i) &= \sin(j/(10000^{2i/d_{\text{model}}})) \\ PE(j, i+1) &= \cos(j/(10000^{2i/d_{\text{model}}})) \end{aligned} \quad (8)$$

where j has values from 0 up to the maximum length of the input sequence minus 1, and i can assume values from 0 up to $d_{\text{model}} - 1$. In our case, d_{model} corresponds to the dimension of the real-valued CSI for each slot which is equal to 64. However, differently from the implementations in [12], [17], we consider the Pre-LN, instead of the Post-LN, see [24] for more details. Additionally, for the encoder model, we consider the *reversed* positional embedding. Intuitively, this means that we start counting the CSI snapshots in the encoder from the last known snapshot. For example, if the input sequence has $\ell = 16$, after having obtained the positional embeddings as described in Eq. (8), we flip them as $PE(15, :) \leftarrow PE(0, :)$, $PE(14, :) \leftarrow PE(1, :)$, etc. This has shown a great impact regarding the generalization property of the TNN. Finally, to improve the performance and reduce overfitting in the TNN, we apply in the encoder the column-wise “DropAttention” regularization to the weight matrix that results from the outer product of the queries and keys, which has been proposed

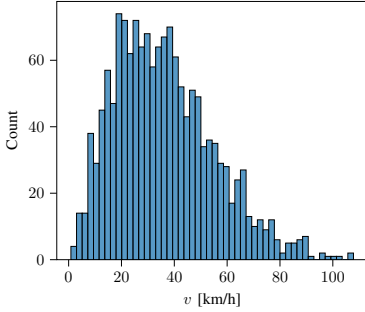


Figure 5. Velocity histogram.

in [25]. Also in this case, we consider a real-valued neural network. Therefore, the CSI is transformed into real-values as described in Subsection III-B, see (4).

IV. SIMULATION RESULTS

For the simulations, we consider CSI sequences generated with QuaDRiGa v.2.6, see [26]. In particular, we generate $N_{\text{samples}} = 150,000$ CSI sequences corresponding to 1500 different velocities. Therefore, we have 100 users for each velocity. Every CSI sequence corresponds to a frame which contains $N_{\text{slot}} = 20$ slots, each with duration $T_{\text{slot}} = 0.5$ ms. The carrier frequency is 2.6 GHz and each velocity v measured in m/s is Rayleigh distributed: $\frac{v}{\gamma^2} \exp\left(-\frac{v^2}{2\gamma^2}\right)$, where $\gamma = 8$. In Fig. 5, for convenience, we show the distribution of the different 1500 velocity realizations measured in km/h. The scenario is the “BERLIN_UMa_NLOS” which generates non-line-of-sight channels with 25 paths. The BS positioned at a height of 25 m is equipped with a uniform rectangular array with $M = 32$ antennas, with 8 vertical and 4 horizontal antenna elements. The users’ initial positions are randomly distributed over a sector of 120 deg, and with a minimum and maximum distance from the BS of 50 m and 150 m, respectively, and at a height of 1.5 m. All the generated CSI sequences are first normalized by the path-gain, and subsequently, they are split into training, validation, and test set with a percentage of 80%, 10%, and 10%, respectively. We consider different noise levels for our simulations. In particular, we corrupt the channel \mathbf{h}_i as described in Eq. (2) according to a noise variance σ_n^2 which fulfills a certain average SNR level. Therefore, given the average SNR we can determine σ_n using the formula

$$\text{SNR} = \frac{\frac{1}{N_{\text{samples}} N_{\text{slot}}} \sum_{j=1}^{N_{\text{samples}}} \sum_{i=1}^{N_{\text{slot}}} \|\{\mathbf{h}_i\}_j\|^2}{M \sigma_n^2}. \quad (9)$$

For our simulations, we assume that the first $\ell = 16$ noisy CSI realizations are known. Therefore, the goal is to predict the next $\delta = 4$ noisy CSI vectors. By defining with $\tilde{\mathbf{H}} = [\tilde{\mathbf{h}}_{\ell+1}, \dots, \tilde{\mathbf{h}}_{\ell+\delta}]$ the real matrix that consists of the noisy CSI snapshots and with $\hat{\mathbf{H}} = [\hat{\mathbf{h}}_{\ell+1}, \dots, \hat{\mathbf{h}}_{\ell+\delta}]$ the real matrix that consists of the predicted CSI snapshots, the average element-wise Huber loss between $\tilde{\mathbf{H}}$ and $\hat{\mathbf{H}}$ is used to train all the

networks. The Huber loss between two scalars is described in Eq. (10) with $\Delta = 1$.

$$\mathcal{L} = \begin{cases} 0.5(x - \hat{x})^2 & \text{if } |x - \hat{x}| < \Delta \\ \Delta(|x - \hat{x}| - 0.5\Delta) & \text{otherwise.} \end{cases} \quad (10)$$

All the models, except the MAR model, are trained for the different average SNR values for a maximum of 1000 epochs with a batch size equal to 200. The Adam optimizer (see [27]) with initial learning rate equal to 10^{-3} is used. The performance metric that we consider is the normalized mean squared error (NMSE) with respect to the test set between the true noiseless CSI and the CSI predicted by the different models using the noisy observations of the previous slots. In formulas, we have:

$$\text{NMSE} = \frac{1}{N_{\text{test}}} \sum_{j=1}^{N_{\text{test}}} \|\mathbf{H}_j - \hat{\mathbf{H}}_j\|_{\text{F}}^2 / \|\mathbf{H}_j\|_{\text{F}}^2 \quad (11)$$

where $\mathbf{H} = [\mathbf{h}_{\ell+1}, \dots, \mathbf{h}_{\ell+\delta}]$ is the matrix that consists of the clean CSI snapshots. To prevent overfitting, during the training, we measure the mean squared error (MSE), with respect to the validation set, between the noisy CSI and the predicted one to determine whether to decrease the learning rate of the optimizer or to stop training the model. In particular, we set the patience of the early-stopping criterion to 30 epochs, which means that if the MSE does not improve by 10^{-4} for 30 epochs, we stop training our model. On the other hand, if the MSE does not improve for 7 epochs we scale the current learning rate of the optimizer by 0.3. Note that the clean CSI is only used during the testing phase to evaluate the performance, whereas for both the training and the MSE evaluation, only noisy CSI observations are used.

Regarding the model parameters, we have used a two-layer MLP, as described in Subsection III-B where the observed dimension, the hidden dimension, and the output dimension are 1024, 512, and 256, respectively. For the LSTM model, described in Subsection III-C, we have considered a two-layer LSTM, hidden states with 128 units, and a final linear layer which maps the last hidden state to the output dimension which is equal to 256. The dimensions of all the weight matrices and bias vectors in Eq. (6) can be easily inferred with the given information. For the Seq2Seq model described in Subsection III-D, we consider GRUs with two layers and hidden states with dimension equal to 128. In the decoder, the first linear layer followed by the softmax activation maps $(64 + 128)$ units to ℓ_{max} units, where 64 is the input dimension (the dimension of \mathbf{h}_i), 128 is the dimension of the hidden state \mathbf{u}_i , ℓ_{max} is the maximum length allowed for the encoder output, e.g., 20, and the addition is due to the concatenation of the two. By following the same reasoning as for the *reversed* positional embedding in the TNN, encoder output sequences of the maximum length will use all the attention weights, while shorter sequences will only use the last few. On the other hand, the second linear layer followed by a ReLU maps $(64 + 128)$

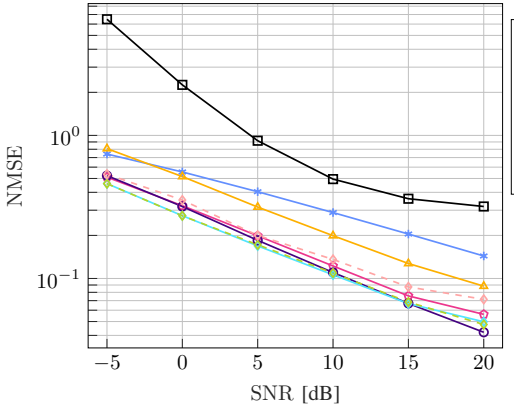


Figure 6. NMSE vs. average SNR. $\ell = 16, \delta = 4$ (Same lengths used for training).

units to 64 units, where 128 is the resulting dimension after the softmax operation and the subsequent multiplication. The decoder’s final linear layer, which produces the CSI prediction for the next step, maps the 128 units of the next hidden state to the 64 units of the next CSI. The dimensions of all the weights matrices and bias vectors of the GRU, that appear in Eq. (7) can be derived with the given information. The TNN described in Subsection III-E has $L_{\text{enc}} = L_{\text{dec}} = 2$, $H = 4$ attention heads in the multi-head attention block, and $d = 16$ such that $Hd = 64$, which is the observed dimension corresponding to the real-valued CSI snapshot. The MLP block in both the encoder and the decoder network contains two linear layers separated by a GeLU non-linearity with a hidden dimension equal to 128. For the column-wise DropAttention module, we opted for a dropout probability of 0.2 and for a window size equal to 1. Note that, out of all the NNs examined in this work, the TNN is the one with the smallest number of parameters.

In Fig. 6, the NMSE vs. average SNR is displayed for all the models described within this work. In particular, we can see that all the models outperform the “Keep-last” setup, in which the last known noisy CSI snapshot is kept for all the δ subsequent snapshots. Additionally, we can observe that the models designed for sequential data, such as LSTM, Seq2Seq, and TNN, outperforms both the MAR and the MLP models. Moreover, both, the Seq2Seq and TNN models, which include an attention mechanism, outperform the LSTM model, despite the fact that the LSTM predict all the δ snapshots in one step. This means that in the LSTM an imperfect prediction for the $\ell + 1$ snapshot has no influence regarding the prediction of the future $\delta - 1$ snapshots. Additionally, the results of both the TNN with the encoder standard positional embedding of [12] and the TNN-Parallel architecture proposed in [13] are displayed. In particular, we can observe that the former has almost exactly the same performance as our TNN, whereas the latter cannot outperform the LSTM. First of all, both the TNN-Parallel and the LSTM predict all the next δ snapshots in one step, rather

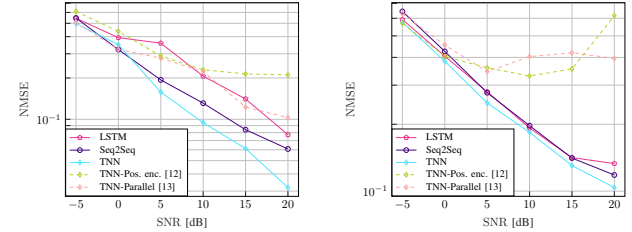


Figure 7. NMSE vs. average SNR. Generalization to lengths different from training.

than sequentially. However, the proposed LSTM has more degrees of freedom, or equivalently more parameters to perform this prediction, due to the final linear layer. On the contrary, in the TNN-Parallel, the parameters for predicting each single CSI snapshot are shared. Secondly, to enable the parallel prediction, the authors in [13] initialize the decoder input with a certain number of historical CSI snapshots, in our case 8, followed by snapshots initialized as all-zeros vectors. On one hand, this prohibits the prediction error propagation, on the other hand, this prevents the transformer decoder to attend also the newest predicted CSI snapshots in order to predict the next one. On the contrary, we observe that both the proposed TNN and the one of [12], in spite of having less parameters than the LSTM, can leverage the predicted CSI snapshots to make better prediction for the next one. As a further benchmark, we observe how the sequential models generalize to sequence lengths different from the ones they were trained on. As shown in Fig. 7, the proposed TNN with reversed encoder positional embedding outperforms all the other models for both the cases in which shorter CSI sequences and longer CSI sequences must be predicted compared to the lengths with respect to which the model was trained. In particular, when comparing the results achieved by our TNN vs. the results achieved with the TNNs with the standard encoder positional embedding, we can observe that the proposed reversed positional embedding for the encoder has a remarkable impact regarding the generalization capabilities of the TNN. Finally, for the sake of completeness, in Fig. 8 we track different quantities during the training of the TNN model for SNR = 5 dB. In particular, both Fig. 8a and 8b show that during training, the MSE for the validation set has a trend similar to the NMSE of the test set measured with respect to both the noisy and the clean data. Additionally, the training Huber loss has similar behavior. Note that the results of the MSE of the validation set are displayed on a different figure because of the different order of magnitude compared to the other quantities.

V. CONCLUSIONS

We have shown that attention-based models such as Seq2Seq and TNNs outperforms RNNs, feed-forward NNs and classical AR models for the task for multi-step CSI prediction. We then have established that by replacing the positional embedding

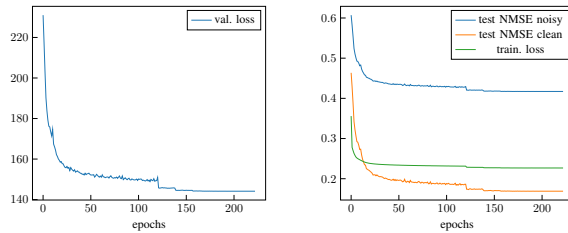


Figure 8. Losses vs. epochs for average SNR = 5 dB of the TNN model.

with the reversed positional embedding in the transformer encoder, extrapolation to different lengths can be enabled in TNNs. In addition, the proposed TNN achieves better results than other models in terms of generalization to CSI sequence lengths that were never seen by the model during training.

REFERENCES

- [1] K. E. Baddour and N. C. Beaulieu, “Autoregressive modeling for fading channel simulation,” *IEEE Trans. Wirel. Commun.*, vol. 4, no. 4, pp. 1650–1662, 2005. [Online]. Available: <https://doi.org/10.1109/TWC.2005.850327>
- [2] A. Barbieri, A. Piemontese, and G. Colavolpe, “On the ARMA approximation for fading channels described by the Clarke model with applications to Kalman-based receivers,” *IEEE Trans. Wirel. Commun.*, vol. 8, no. 2, pp. 535–540, 2009. [Online]. Available: <https://doi.org/10.1109/TWC.2009.070188>
- [3] A. H. E. Husseini, E. P. Simon, and L. Ros, “Optimization of the second order autoregressive model AR(2) for Rayleigh-Jakes flat fading channel estimation with Kalman filter,” in *22nd International Conference on Digital Signal Processing, DSP 2017, London, United Kingdom, August 23-25, 2017*. IEEE, 2017, pp. 1–5. [Online]. Available: <https://doi.org/10.1109/ICDSP.2017.8096103>
- [4] T. Zemen, C. F. Mecklenbrauker, F. Kaltenberger, and B. H. Fleury, “Minimum-Energy Band-Limited Predictor With Dynamic Subspace Selection for Time-Variant Flat-Fading Channels,” *IEEE Transactions on Signal Processing*, vol. 55, no. 9, pp. 4534–4548, 2007.
- [5] J. Yuan, H. Q. Ngo, and M. Matthaiou, “Machine Learning-Based Channel Prediction in Massive MIMO with Channel Aging,” *IEEE Transactions on Wireless Communications*, vol. 19, no. 5, pp. 2960–2973, 2020.
- [6] K. Pratik, R. A. Amjad, A. Behboodi, J. B. Soriaga, and M. Welling, “Neural Augmentation of Kalman Filter with Hypernetwork for Channel Tracking,” *2021 IEEE Global Communications Conference, GLOBECOM 2021 - Proceedings*, 2021.
- [7] S. Park and O. Simeone, “Predicting Flat-Fading Channels via Meta-Learned Closed-Form Linear Filters and Equilibrium Propagation,” 2022. [Online]. Available: <https://arxiv.org/abs/2203.12715>
- [8] W. Jiang, M. Strufe, and H. D. Schotten, “Long-Range MIMO Channel Prediction Using Recurrent Neural Networks,” in *IEEE 17th Annual Consumer Communications & Networking Conference, CCNC 2020, Las Vegas, NV, USA, January 10-13, 2020*. IEEE, 2020, pp. 1–6. [Online]. Available: <https://doi.org/10.1109/CCNC46108.2020.9045219>
- [9] M. K. Shehzad, L. Rose, S. Wesemann, M. Assaad, and S. A. Hassan, “Design of an Efficient CSI Feedback Mechanism in Massive MIMO Systems: A Machine Learning Approach using Empirical Data,” *CoRR*, vol. abs/2208.11951, 2022. [Online]. Available: <https://doi.org/10.48550/arXiv.2208.11951>
- [10] R. Pascanu, T. Mikolov, and Y. Bengio, “On the difficulty of training recurrent neural networks,” in *Proceedings of the 30th International Conference on Machine Learning, ICML 2013, Atlanta, GA, USA, 16-21 June 2013*, ser. JMLR Workshop and Conference Proceedings, vol. 28. JMLR.org, 2013, pp. 1310–1318. [Online]. Available: <http://proceedings.mlr.press/v28/pascanu13.html>
- [11] M. Chu, A. Liu, C. Jiang, V. K. N. Lau, and T. Yang, “Wireless Channel Prediction for Multi-user Physical Layer with Deep Reinforcement Learning,” in *2022 IEEE 95th Vehicular Technology Conference: (VTC2022-Spring)*, 2022, pp. 1–5.
- [12] A. Vaswani, N. Shazeer, N. Parmar, J. Uszkoreit, L. Jones, A. N. Gomez, L. Kaiser, and I. Polosukhin, “Attention is All you Need,” in *Advances in Neural Information Processing Systems 30: Annual Conference on Neural Information Processing Systems 2017, December 4-9, 2017, Long Beach, CA, USA*, 2017, pp. 5998–6008.
- [13] H. Jiang, M. Cui, D. W. K. Ng, and L. Dai, “Accurate Channel Prediction Based on Transformer: Making Mobility Negligible,” *IEEE Journal on Selected Areas in Communications*, vol. 40, no. 9, pp. 2717–2732, 2022.
- [14] Y. Xu, M. Yuan, and M.-O. Pun, “Transformer Empowered CSI Feedback for Massive MIMO Systems,” in *2021 30th Wireless and Optical Communications Conference (WOCC)*, 2021, pp. 157–161.
- [15] Y. Cui, A. Guo, and C. Song, “Transnet: Full attention network for csi feedback in fdd massive mimo system,” *IEEE Wireless Communications Letters*, vol. 11, no. 5, pp. 903–907, 2022.
- [16] V. Rizzello, H. Zhang, M. Joham, and W. Utschick, “Compression Techniques for MIMO Channels in FDD Systems,” in *2022 IEEE Data Science and Learning Workshop (DSLW)*, 2022, pp. 1–6.
- [17] N. Wu, B. Green, X. Ben, and S. O’Banion, “Deep Transformer Models for Time Series Forecasting: The Influenza Prevalence Case,” *CoRR*, vol. abs/2001.08317, 2020. [Online]. Available: <https://arxiv.org/abs/2001.08317>
- [18] S. Hochreiter and J. Schmidhuber, “Long Short-Term Memory,” *Neural Computation*, vol. 9, no. 8, pp. 1735–1780, 11 1997. [Online]. Available: <https://doi.org/10.1162/neco.1997.9.8.1735>
- [19] I. Sutskever, O. Vinyals, and Q. V. Le, “Sequence to Sequence Learning with Neural Networks,” in *Advances in Neural Information Processing Systems 27: Annual Conference on Neural Information Processing Systems 2014, December 8-13 2014, Montreal, Quebec, Canada*, 2014, pp. 3104–3112.
- [20] D. Bahdanau, K. Cho, and Y. Bengio, “Neural Machine Translation by Jointly Learning to Align and Translate,” in *3rd International Conference on Learning Representations, ICLR 2015, San Diego, CA, USA, May 7-9, 2015, Conference Track Proceedings*, 2015.
- [21] R. J. Williams and D. Zipser, “A learning algorithm for continually running fully recurrent neural networks,” *Neural Comput.*, vol. 1, no. 2, pp. 270–280, 1989. [Online]. Available: <https://doi.org/10.1162/neco.1989.1.2.270>
- [22] J. L. Ba, J. R. Kiros, and G. E. Hinton, “Layer Normalization,” 2016. [Online]. Available: <https://arxiv.org/abs/1607.06450>
- [23] D. Hendrycks and K. Gimpel, “Gaussian Error Linear Units (GELUs),” 2016. [Online]. Available: <https://arxiv.org/abs/1606.08415>
- [24] R. Xiong, Y. Yang, D. He, K. Zheng, S. Zheng, C. Xing, H. Zhang, Y. Lan, L. Wang, and T. Liu, “On Layer Normalization in the Transformer Architecture,” in *Proceedings of the 37th International Conference on Machine Learning, ICML 2020, 13-18 July 2020, Virtual Event*, ser. Proceedings of Machine Learning Research, vol. 119. PMLR, 2020, pp. 10 524–10 533.
- [25] Z. Lin, P. Liu, L. Huang, J. Chen, X. Qiu, and X. Huang, “DropAttention: A Regularization Method for Fully-Connected Self-Attention Networks,” *CoRR*, vol. abs/1907.11065, 2019. [Online]. Available: <http://arxiv.org/abs/1907.11065>
- [26] S. Jaeckel, L. Raschkowski, K. Boerner, and L. Thiele, “QuaDRiGa: A 3-D Multi-Cell Channel Model With Time Evolution for Enabling Virtual Field Trials,” *IEEE Transactions on Antennas and Propagation*, vol. 62, no. 6, pp. 3242–3256, 2014.
- [27] D. P. Kingma and J. Ba, “Adam: A Method for Stochastic Optimization,” in *3rd International Conference on Learning Representations, ICLR 2015, San Diego, CA, USA, May 7-9, 2015, Conference Track Proceedings*, 2015. [Online]. Available: <http://arxiv.org/abs/1412.6980>